

N 62 71041

NASA TN D-467

NASA TN D-467



11V-20

3-0131

TECHNICAL NOTE

D-467

PERFORMANCE OF SEVERAL CONICAL CONVERGENT-DIVERGENT

ROCKET-TYPE EXHAUST NOZZLES

By C. E. Campbell and J. M. Farley

Lewis Research Center
Cleveland, Ohio

NATIONAL AERONAUTICS AND SPACE ADMINISTRATION

WASHINGTON

September 1960

-

-

-

-

-

-

NATIONAL AERONAUTICS AND SPACE ADMINISTRATION

TECHNICAL NOTE D-467

PERFORMANCE OF SEVERAL CONICAL CONVERGENT-DIVERGENT

ROCKET-TYPE EXHAUST NOZZLES

By C. E. Campbell and J. M. Farley

SUMMARY

An investigation was conducted to obtain nozzle performance data with relatively large-scale models at pressure ratios as high as 120. Conical convergent-divergent nozzles with divergence angles α of 15°, 25°, and 29° were each tested at area ratios of approximately 10, 25, and 40. Heated air (1200° F) was supplied at the nozzle inlet at pressures up to 145 pounds per square inch absolute and was exhausted into quiescent air at pressures as low as 1.2 pounds per square inch absolute.

Thrust ratios for all nozzle configurations are presented over the range of pressure ratios attainable and were extrapolated when possible to design pressure ratio and beyond. Design thrust ratios decreased with increasing nozzle divergence angle according to the trend predicted by the $(1 + \cos \alpha)/2$ parameter. Decreasing the nozzle divergence angle resulted in sizable increases in thrust ratio for a given surface-area ratio (nozzle weight), particularly at low nozzle pressure ratios.

Correlations of the nozzle static pressure at separation and of the average static pressure downstream of separation with various nozzle parameters permitted the calculation of thrust in the separated-flow region from unseparated static-pressure distributions. Thrust ratios calculated by this method agreed with measured values within about 1 percent.

INTRODUCTION

Although exhaust-nozzle design-point performance has been experimentally and theoretically well established, off-design performance, especially in the overexpanded separated region, is more difficult to ascertain and is not completely amenable to analysis. The wide range of exhaust pressures encountered by missiles and spacecraft results in a considerable amount of off-design engine operating time. Because of the sensitivity of vehicle performance to nozzle efficiency (particularly

E-481

CD-1

payload), some knowledge of off-design performance is necessary to determine accurately the overall vehicle flight history. Although there have been a number of design and off-design investigations of convergent-divergent exhaust nozzles, most of them have been either full-scale rocket-engine tests with their inherent measurement limitations, or relatively cold gas tests with small-scale models at pressure ratios of less than 50.

In order to extend the preciseness of experimental nozzle performance data (especially in the off-design region), the investigation presented in this report was conducted with relatively large-scale models (6.5-in. throat diam.), a gas temperature of 1200° F, and pressure ratios from 4 to 120. Three basic nozzles were used having nominal divergence half-angles of 15°, 25°, and 29°. Each nozzle was built and operated with an area ratio of 40 and then cut off for tests with area ratios of about 25 and 10. Although the bulk of the data were obtained with an inlet-air temperature of about 1200° F, some data were obtained with unheated air. The use of direct-fired heaters to raise the inlet temperature resulted in the presence of condensation shock in the nozzles during most of the heated-air testing; however, it was possible to correct the data for this effect.

Thrust ratios are presented for all nozzle configurations over a range of nozzle pressure ratios from 10 to 100 and were extrapolated when possible up to a pressure ratio of 1000. Design thrust ratios are compared with expected values from the $(1 + \cos \alpha)/2$ parameter of reference 1, and the performances of the different-divergence-angle nozzles are compared on the basis of nozzle surface area (weight). A simplified method of thrust determination is developed that permits the calculation of nozzle thrust in the separated-flow region from unseparated static-pressure profiles.

APPARATUS

The three basic nozzle configurations investigated (fig. 1) had inlet diameters of 9 inches, nominal throat diameters of 6.5 inches, overall area ratios of 40, and divergence half-angles of approximately 15°, 25°, and 29°. The original nozzles were subsequently cut off to give area ratios of about 25 and 10, which resulted in a total of nine different nozzle configurations. All nozzles were of stainless-steel construction and contained static wall orifices with approximately 2-inch axial spacing throughout their lengths. Detailed nozzle dimensions are given in the sketches of figure 1, and the more important nozzle criteria are summarized in the following table:

Divergence angle, α , deg	Throat diam., in.	Area ratio, A_e/A_{cr}
15.3	6.49	9.2 24.5 40.1
25.0	6.50	9.9 24.3 40.0
29.0	6.49	10.5 28.9 40.1

A sketch of the nozzle rig is shown in figure 2. The nozzle assembly was rigidly mounted on a flexure-plate-supported test platform that was connected by a linkage to a calibrated null-type thrust cell. Dry air (1 grain/lb) entered the nozzle assembly through a bellmouth Venturi duct in which mass-flow measurements were made. The air then passed through five combustor cans before entering the nozzle inlet. (During cold-flow operation, the combustor cans were removed from the combustor section.) A labyrinth seal just downstream of the bellmouth inlet mechanically isolated the nozzle and associated ducting from the inlet-air line, thus permitting measurement of the thrust forces.

TEST PROCEDURE

Nozzle performance data were obtained with each configuration at nozzle-inlet pressures of about 145, 90, and 50 pounds per square inch absolute to determine the effects of Reynolds number on nozzle performance. The exhaust pressure was varied from about 1.2 to 12 pounds per square inch, which gave a range of nozzle pressure ratios from 4 to 120. The exhaust pressure was varied in both increasing and decreasing directions to check for possible hysteresis in the thrust-measuring system. The nozzle-inlet air temperature was maintained at approximately 1200° F by burning JP fuel in the five combustor cans upstream of the nozzle inlet. Although the facility inlet air was dried to about 1 grain per pound, the combustion of fuel increased the moisture content so that condensation shocks occurred in the nozzle during most of the heated-air testing. Some cold-flow data (80° F air temp.) were also obtained, which were essentially free of condensation shock. During these cold-flow tests, the maximum nozzle pressure ratio available was about 77.

DATA PROCEDURE

Measured Thrust

Nozzle thrust F was determined over the available pressure-ratio range from the summation of momentum and pressure forces on the installation and the thrust-bed balance force as measured by the thrust-measuring cell. Nozzle thrust coefficient C_F was obtained by dividing the measured thrust F by the product of nozzle-inlet total pressure, nozzle throat area, and the throat flow coefficient ϕ . A throat flow-coefficient value of 0.98 was determined during cold-flow tests from the ratio of actual airflow to airflow as calculated from nozzle-inlet pressure and temperature measurements and assumed sonic conditions at the nozzle throat. Nozzle thrust ratio F/F_{id} was obtained by dividing the measured thrust F by the product of actual mass flow and the ideal velocity that would be obtained with isentropic expansion from nozzle-inlet conditions to ambient pressure. (All symbols are defined in appendix A.)

Corrected Thrust

Although the facility inlet air was dried to about 1 grain per pound, the use of direct-fired heaters to raise the nozzle-inlet temperature caused the moisture content to increase to about 133 grains per pound. This resulted in condensation shocks in the nozzles at an area ratio of about 8 except when flow separation occurred upstream of this area ratio. All the affected measured-thrust values were corrected for condensation-shock effects by comparing integrated-pressure thrust calculations from measured nozzle pressure distributions with those from the calculated nozzle pressure distributions that would have occurred without condensation shock. (The unseparated pressure distributions without condensation shock were determined by the method described in appendix B.) Calculated shock-free pressure distributions were necessary because measured shock-free data (cold flow) were not obtained with all nozzle configurations and did not cover a large enough range of nozzle pressure ratio. Condensation-shock-free thrust calculations for the nozzle operating in the separated-flow region (separation and oblique shock within the nozzle) were made possible by the correlation of the nozzle static pressure at separation and the average nozzle static pressure downstream of the separation point with various nozzle parameters. The performance of nozzle configurations for which the condensation-shock-free unseparated static-pressure distribution could be determined out to the nozzle exit was extrapolated to design pressure ratio and beyond. This was possible because the total momentum at the nozzle exit is constant for all pressure ratios beyond that required for full flow, and thus overall thrust varies directly with nozzle pressure ratio.

RESULTS AND DISCUSSION

Effects of Condensation Shock

E-481

Comparison of measured and corrected thrust. - Actual thrust-ratio data and corrected thrust-ratio values obtained at three different area ratios with the 29° nozzle are shown in figure 3 as a function of nozzle pressure ratio. It can be seen that the presence of condensation shock resulted in lower values of thrust ratio in the overexpanded region of about 1 percent for the nozzles with area ratios of 25 and 40 and had negligible effect on the area-ratio-10 nozzle. Cold-flow data (fig. 3(b)), which were essentially free of condensation shock, agreed well with the shock-free calculated curve. Condensation shock also lowered the pressure ratio at which full flow is attained, thereby resulting in incorrect values of design-point pressure ratio and design thrust ratio. The effect of condensation shock on the thrust performance of the 15° and 25° nozzles was essentially the same as shown for the 29° nozzles. The effect of inlet pressure level (Reynolds number) on thrust performance is seen to be within the overall scatter of the data. The various effects of condensation shock on nozzle performance were eliminated by a method developed later in this report.

Comparison of measured and corrected pressure distributions. - The static-pressure distribution of the 29° nozzle is shown in figure 4. The diagonal solid line represents the measured unseparated pressure distribution obtained with this nozzle. The portion of this line between area ratios of 8 and 28 is the distribution after the occurrence of condensation shock. The dashed line just below this portion of the solid line represents the calculated static-pressure distribution that would have occurred without condensation shock. The agreement of the cold-flow data with the calculated shock-free line is, of course, about the same as the agreement in thrust that was evident in figure 3(b).

The static-pressure-ratio rise across the oblique shocks associated with separation (indicated by the nearly vertical lines) was approximately of the same magnitude and location for a given nozzle pressure ratio regardless of the nozzle-inlet total pressure or overall nozzle area ratio A_e/A_{cr} . The reason for the difference in thrust ratio (fig. 3) with and without condensation shock can be discerned from the static-pressure distribution. Although the static pressure up to separation is lower without condensation shock, this is more than offset by the fact that separation occurs farther upstream and results in a larger pressure-area force downstream of separation. Therefore, the net result is a slightly greater thrust for the condensation-shock-free case.

The static-pressure distributions of figure 4 are typical of nozzles exhausting into quiescent air; however, the nozzle tests of reference 2 indicate that, with external flow, the pressure distributions

might be somewhat altered. Since these external-flow tests were conducted with relatively small-area-ratio nozzles and at relatively low pressure ratios, the possible effects of external flow on the pressure-distribution data herein could not be determined.

Thrust Performance

Nozzle performance with the effects of condensation shock eliminated is presented as plots of thrust ratio F/F_{id} against nozzle pressure ratio, nozzle divergence angle, and nozzle surface-area ratio. In those cases where it was possible to establish full flow through the nozzle, the thrust performance was extrapolated to design pressure ratio and beyond.

Pressure ratio. - Thrust ratios for all nozzle configurations investigated are shown in figure 5 as a function of nozzle pressure ratio. Thrust ratios for the 10- and 25-area-ratio nozzles peaked at approximately design pressure ratio (ambient pressure equal to nozzle-exit pressure) and decreased again at higher pressure ratios. Design-point performance could not be determined for the 40-area-ratio nozzles, since the large pressure ratio necessary to establish full flow could not be attained in this investigation. The values of full-flow and design-point pressure ratio for the 29° nozzles (indicated by the vertical ticks) are high relative to the 15° and 25° nozzles, because the area ratios of this nozzle were high compared with the nominal values (see APPARATUS table or fig. 1). The smaller-angle nozzles gave higher thrust ratios at all pressure ratios above about 13. Increasing the nozzle area ratio from 10 to about 25 for a fixed nozzle angle resulted in about the same maximum (design-point) thrust ratio but required a higher nozzle pressure ratio.

Divergence angle. - The nonaxiality of flow at the exit of a conical nozzle results in a thrust loss that should be predictable from the $(1 + \cos \alpha)/2$ parameter of reference 1. Design thrust ratios of the 10- and 25-area-ratio nozzles are shown in figure 6 as a function of nozzle divergence angle α along with the predicted values adjusted about 1/2 percent for boundary-layer losses. Design thrust ratios decreased with increasing α according to the predicted trend, but the absolute values of design thrust ratio were about 1 percent higher than expected. This is attributed to inaccuracies in mass-flow measurement during the determination of flow coefficient, whose value of 0.98 is about 1 percent lower than usually measured for these types of nozzles. All values of thrust ratio and thrust coefficient presented in this report are therefore presumed to be about 1 percent high.

Surface-area ratio. - A comparison of the thrust ratios that can be obtained with the different-divergence-angle nozzles as a function of

surface-area ratio (ratio of divergent surface area to throat area) is shown in figure 7 for pressure ratios of 200, 500, and infinity (exhaust into a vacuum). Surface area was used as a basis of comparison because it is felt to be closely related to nozzle weight for the range of area ratios considered. At a given surface-area ratio, decreasing α from 29° to 15° increased the thrust ratio about 3 percentage points at infinite pressure ratio and as much as 6 points at a pressure ratio of 200. Although the divergence angle for maximum thrust ratio may be lower than 15° , it is generally accepted that 15° gives a good compromise between performance and weight. The nozzle area ratio required for maximum thrust ratio at finite pressure ratios (figs. 7(a) and (b)) can easily be determined from the peaks of the thrust-ratio curves. However, at infinite pressure ratio (fig. 7(c)), which will be approached by upper-stage space rockets, thrust ratios continue to rise with increasing area ratio, and a compromise between desired thrust and nozzle weight or length will be necessary.

Calculated-Thrust Method

The determination of nozzle thrust from internal static-pressure measurements is discussed in the following sections. The thrust-coefficient equation in terms of pressure and momentum forces is

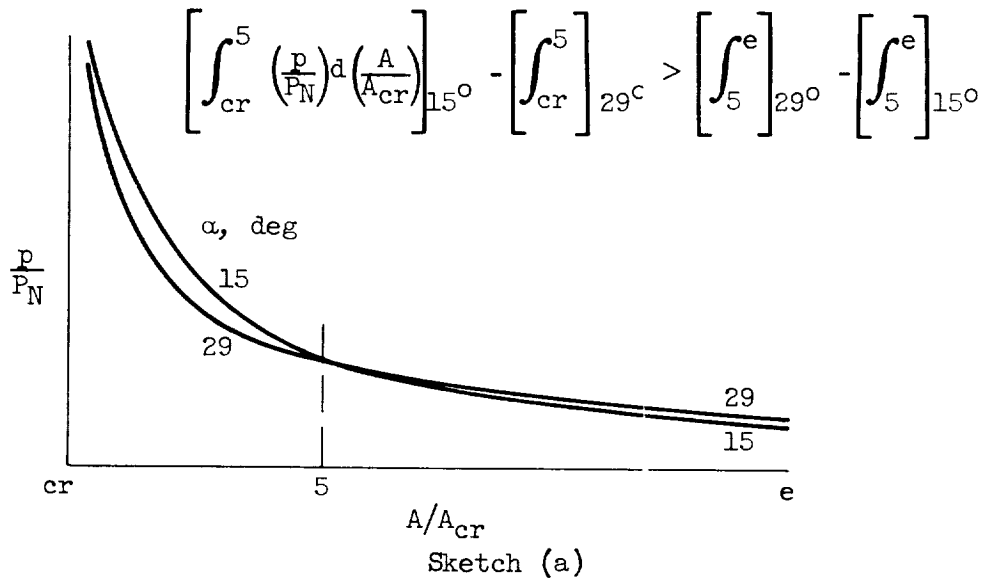
$$C_F = \frac{F}{\phi P_N A_{cr}} = \left[C_{F, cr} + \frac{1}{\phi} \int_{cr}^s \left(\frac{p}{P_N} \right) d \left(\frac{A}{A_{cr}} \right) + \frac{1}{\phi} \int_s^e \left(\frac{p}{P_N} \right) d \left(\frac{A}{A_{cr}} \right) \right] - \frac{1}{\phi} \left(\frac{p_a}{P_N} \right) \left(\frac{A_e}{A_{cr}} \right)$$

where the term in the brackets represents the total momentum at the nozzle exit, or the thrust coefficient of the nozzle discharging into a vacuum. The integrated pressure-area terms would normally be determined from actual nozzle pressure distributions; however, as a means of avoiding this time-consuming process, or in the absence of separated pressure distributions, the integral values can be determined from unseparated pressure distributions and the generalized curves presented herein. The throat thrust-coefficient term $C_{F, cr}$ can be obtained from the theoret-

ical value $\left[2 \left(\frac{\gamma+1}{2} \right)^{-\frac{1}{\gamma-1}} \right]$ and the throat flow coefficient ϕ . However, because of the suspected inaccuracy of the measured flow coefficient, an effective throat thrust coefficient was used in the thrust calculations in order to attribute any differences between measured and calculated thrusts solely to the integration method.

Pressure integration upstream of separation. - Integrations of measured unseparated static-pressure distributions (with condensation shock) and calculated unseparated static-pressure distributions (without

condensation shock) are shown in figure 8 as a function of nozzle area ratio. These curves are valid for any area-ratio station in the nozzle as long as flow separation has not occurred upstream of the area ratio of interest. They also yield directly the full-flow value (\int_{cr}^e) of the force coefficient acting on the divergent portion of a particular size nozzle (A_e/A_{cr}). The higher value of pressure-area force coefficient immediately downstream of the throat of the smaller-angle nozzles is due to the initially less rapid expansion near the throat region (see sketch (a)). Although the static-pressure profiles of the various angle nozzles eventually cross (i.e., the nozzle static pressure of the larger-angle nozzles becomes higher at large area ratios), the slightly higher integrated pressure force in this region does not make up for the initial lower pressure level.



Evaluation of throat thrust coefficient. - The effective throat thrust coefficient $C_{F, cr}$ was determined experimentally from the data (with condensation shock) shown in figure 9. Extrapolation of measured C_F data, obtained at pressure ratios beyond full flow, out to zero ambient pressure ($p_a/P_N = 0$) gives values of C_F in terms of throat thrust coefficient $C_{F, cr}$ and the full-flow integrated pressure-area coefficient of figure 8, so that

$$C_{F, cr} = C_F - \frac{1}{\phi} \int_{cr}^e \left(\frac{p}{P_N} \right) d \left(\frac{A}{A_{cr}} \right)$$

Using the values of C_F at zero pressure and $\frac{1}{\phi} \int_{cr}^e$ from the solid lines of figure 8 (with condensation shock) resulted in an average

experimental value of throat thrust coefficient of 1.246 for the three 10-area-ratio nozzles of 15°, 25°, and 29° half-angle. This value of throat thrust would, of course, also apply to the higher area ratios.

Determination of separation point. - After the throat thrust coefficient is evaluated and the method of determining the integrated pressure-area force up to separation is known, the separation point for a given nozzle pressure ratio is next determined. This is accomplished by making use of the correlation of nozzle static-pressure ratio at separation with nozzle pressure ratio as shown in figure 10. Lines of constant Mach number ratio are included to show the agreement of the separation data with theory. These lines were calculated from information in reference 3 assuming various Mach number ratios with no total-pressure loss (for the condensation-shock-free case) and one-dimensional shock theory. The Mach number ratio lines in the condensation-shock region were calculated with a total-pressure loss of 0.32 due to condensation shock (see appendix B). Various analyses (refs. 4 and 5) have indicated that the Mach number ratio across the oblique shock wave is primarily dependent upon the boundary layer and should be approximately constant at a value of 0.76. Separation data for all nozzle configurations tended to generalize at a Mach number ratio of about 0.76 or 0.77 for both hot and cold flow and for all nozzle pressure ratios for which separation data could be determined. The constant Mach number ratio lines for cold flow ($\gamma = 1.40$) were coincidentally the same as for hot flow ($\gamma = 1.34$) with condensation shock. With this information, it is now possible to determine the separation pressure ratio for any value of nozzle pressure ratio. With the separation conditions known, the area ratio at separation can be determined from pressure-distribution curves such as figure 4, and the integrated pressure-area force prior to separation can be determined from figure 8.

Pressure integration downstream of separation. - The final step in the calculation of nozzle thrust coefficient is to evaluate the force on the downstream portion of the nozzle where the flow is separated. This is simply accomplished with the correlation of figure 11, which shows the relation of the average static pressure downstream of the separation point with nozzle pressure ratio and various other nozzle parameters. It can be seen that the data for all nozzle configurations generalized with reasonable accuracy when the parameter $\left[1 - \left(\frac{\bar{P}_{s-e}}{P_a} \right) \cos\left(\frac{\alpha}{Z}\right) \right]$ was plotted as a function of $\left(\frac{P_a}{P_N} \right) \left(\frac{A_e - A_s}{A_{cr}} \right)$. The term sought for the thrust equation, \int_s^e , is related to the average static-pressure ratio downstream of separation as follows:

$$\int_s^e \left(\frac{p}{P_N} \right) d\left(\frac{A}{A_{cr}} \right) = \left(\frac{\bar{P}_{s-e}}{P_N} \right) \left(\frac{A_e - A_s}{A_{cr}} \right)$$

(3) The integrated pressure-area coefficient from the nozzle throat to the separation point, $\int_{cr}^s \left(\frac{p}{P_N}\right) d\left(\frac{A}{A_{cr}}\right)$, is obtained from A_s/A_{cr} and figure 8.

(4) The integrated pressure-area coefficient from separation point to nozzle exit is obtained from figure 11:

$$\int_s^e \left(\frac{p}{P_N}\right) d\left(\frac{A}{A_{cr}}\right) = \left\{ 1 - \left[1 - \left(\frac{P_{s-e}}{P_a}\right) \cos\left(\frac{\alpha}{2}\right) \right] \right\} \left(\frac{P_a}{P_N}\right) \left(\frac{A_e - A_s}{A_{cr}}\right) \left(\frac{1}{\cos\frac{\alpha}{2}}\right)$$

$$(5) C_F = C_{F,cr} + \frac{1}{\phi} \int_{cr}^s \left(\frac{p}{P_N}\right) d\left(\frac{A}{A_{cr}}\right) + \frac{1}{\phi} \int_s^e \left(\frac{p}{P_N}\right) d\left(\frac{A}{A_{cr}}\right) - \frac{1}{\phi} \left(\frac{P_a}{P_N}\right) \left(\frac{A_e}{A_{cr}}\right).$$

$$(6) \frac{F}{F_{id}} = \frac{C_F P_N A_{cr}}{m V_{id}}$$

where V_{id} is the ideal velocity that would be obtained with isentropic expansion to ambient pressure.

Comparison of measured and calculated thrusts. - A comparison of measured thrust ratios in the separated-flow region with values calculated by the preceding method is shown in figure 12 for the three different-divergence-angle nozzles at a different area ratio. Calculated thrusts agreed within 1 percent of the measured values for pressure ratios from the full-flow value down to about 6 for the 10- and 25-area-ratio nozzles and down to about 15 for the 40-area-ratio nozzle. This more than covers the overexpanded region of practical interest and also the region in which condensation-shock corrections were necessary. Thus, the correlations of figures 10 and 11 permit the calculation of thrust for any conical convergent-divergent nozzle as long as the unseparated static-pressure distribution is known throughout the nozzle.

SUMMARY OF RESULTS

The results of a performance investigation of several conical convergent-divergent rocket-type nozzles are as follows:

1. Design thrust ratios decreased with increasing nozzle divergence angle according to the trend predicted by the $(1 + \cos \alpha)/2$ parameter.
2. Decreasing the nozzle divergence angle to about 15° resulted in a sizable increase in thrust ratio for a given surface-area ratio (nozzle weight), particularly at low nozzle pressure ratios.

3. Correlations of the nozzle static pressure at separation and of the average static pressure downstream of separation with various nozzle parameters permitted the calculation of thrust in the separated-flow region from unseparated static-pressure distributions. Thrust ratios calculated by this method agreed with measured values within about 1 percent.

Lewis Research Center
National Aeronautics and Space Administration
Cleveland, Ohio, May 20, 1960

APPENDIX A

SYMBOLS

A	area, sq ft
C_F	thrust coefficient, $F/\phi A_{cr} P_N$
F	nozzle thrust, lb
F/F_{id}	thrust ratio
F_{id}	ideal thrust, $\phi w_{cr} V_{id}/g$, lb
g	acceleration due to gravity, 32.17 ft/sec ²
M	Mach number
m	mass flow, w_{cr}/g
P	total pressure, lb/sq ft abs
p	static pressure, lb/sq ft abs
T	total temperature, °R
V	velocity, ft/sec
w	airflow, lb/sec
α	nozzle divergence angle, deg
γ	ratio of specific heats
ϕ	flow coefficient, w_1/w_{cr}

Subscripts:

a	ambient (exhaust section)
cr	throat or critical ($M = 1$) conditions
e	nozzle exit
id	ideal
N	nozzle inlet

14

S surface
s separation point
x bellmouth inlet
O inlet-air line
l airflow measuring station

APPENDIX B

CORRECTION OF MEASURED STATIC-PRESSURE DISTRIBUTIONS WITH CONDENSATION

SHOCK TO DISTRIBUTIONS WITHOUT CONDENSATION SHOCK

E-481

The use of combustion-type heaters to raise the inlet-air temperature resulted in a nozzle-inlet moisture content of about 133 grains per pound. Data of reference 6 indicate that, with this moisture content and inlet-air conditions of 1200° F and 145 pounds per square inch absolute, moisture condensation would initiate at a Mach number of about 3.65. The condensation is, of course, accompanied by heat release, which causes a total-pressure loss (shock) and a static-pressure increase downstream of the condensation region. Measured static-pressure distributions were corrected for condensation shock by subtracting the difference in static-pressure distributions with and without condensation shock calculated for the ideal one-dimensional-flow case ($\gamma = 1.4$). The methods and assumptions used to calculate the static-pressure correction are as follows:

(1) It was assumed that the flow initially expanded to a condition of supersaturation and then, at the conditions prescribed by reference 6, shocked to equilibrium (saturation) conditions. It was further assumed that equilibrium flow existed throughout the remainder of the expansion (moisture condensed at a rate to maintain saturation conditions). From this rate of moisture condensation with Mach number, the variation of total temperature with Mach number was calculated from the heat of vaporization of the water.

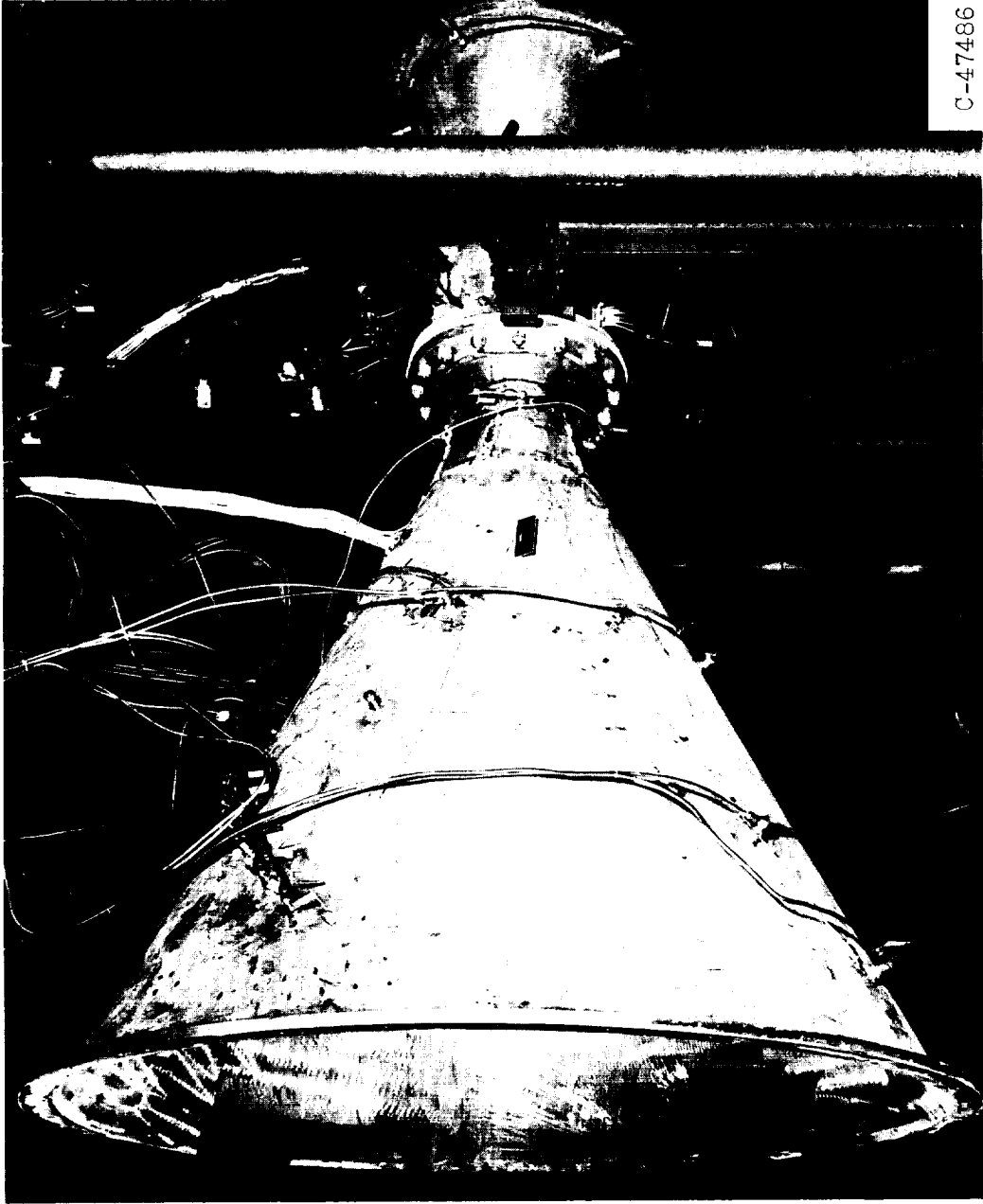
(2) The variation of total pressure in the condensation-shock region P'/P_N with Mach number was approximated by calculating the total-pressure loss due to heat addition at constant area for small increments of Mach number and temperature-rise ratio. The overall total-pressure-loss ratio through the condensation-shock region was determined to be about 0.32.

(3) The variation of static pressure in the condensation-shock region p'/P_N with Mach number was obtained by multiplying the one-dimensional static-pressure ratio for a given Mach number by P'/P_N . The area ratio A'/A_{cr} corresponding to this Mach number was determined by multiplying the one-dimensional area ratio by the ratio $A'/A = P\sqrt{T'}/P'\sqrt{T}$ as required by continuity. This gave the static-pressure distribution with condensation shock, p'/P_N against A'/A_{cr} , for the one-dimensional-flow case.

(4) The difference between the calculated static-pressure distribution with condensation shock (p'/P_N against A'/A_{cr}) and the one-dimensional static-pressure distribution (p/P_{II} against A/A_{cr}) was employed as a correction factor by subtracting it from the measured static-pressure distributions. This then established the static-pressure distributions that would have occurred in the nozzles if there had been no condensation shock.

REFERENCES

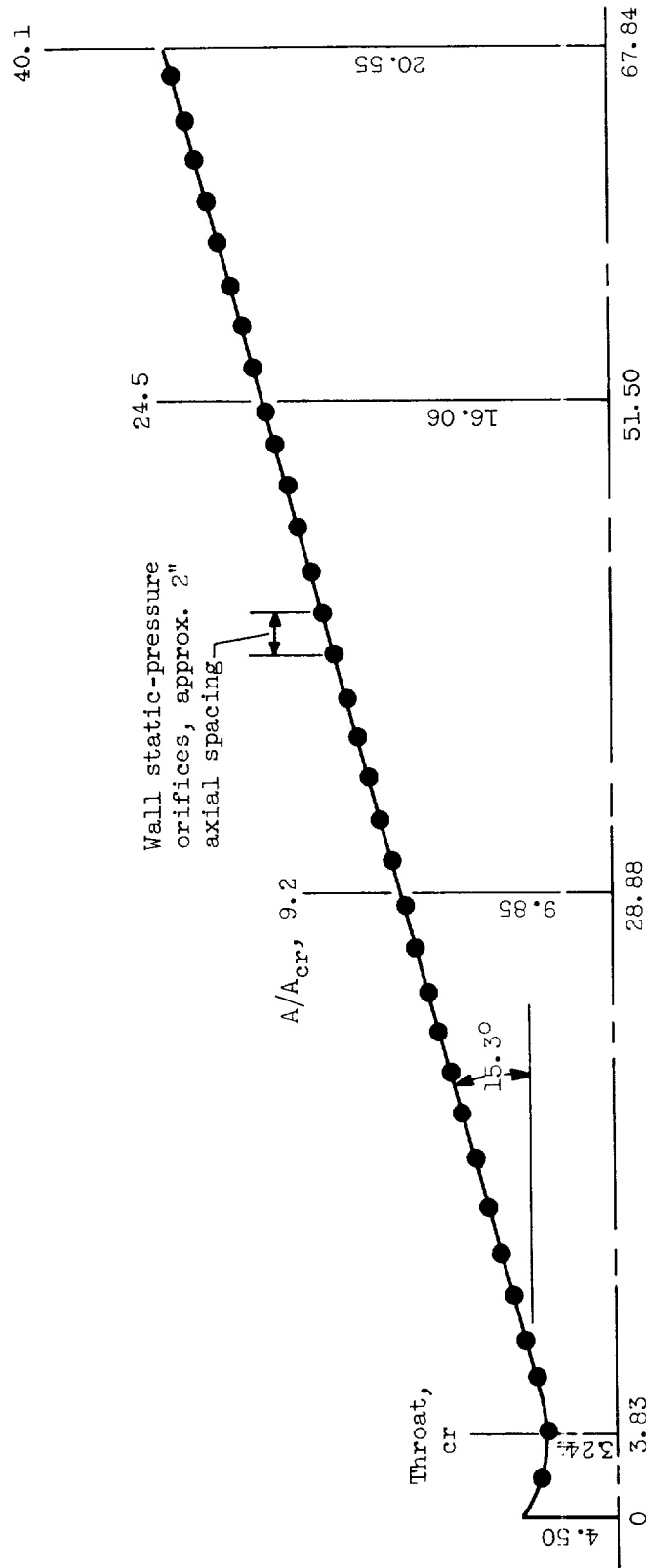
1. Englert, Gerald W., and Kochendorfer, Fred D.: Estimated Performance of Radial-Flow Exit Nozzles for Air in Chemical Equilibrium. NASA MEMO 1-5-59E, 1959.
2. Musial, N. T., and Ward, James J.: Overexpanded Performance of Conical Nozzles with Area Ratios of 6 and 9 With and Without Supersonic External Flow. NASA TM X-83, 1959.
3. Ames Research Staff: Equations, Tables, and Charts for Compressible Flow. NACA Rep. 1135, 1953. (Supersedes NACA TN 1428.)
4. Reshotko, Eli, and Tucker, Maurice: Effect of a Discontinuity on Turbulent Boundary-Layer-Thickness Parameters with Application to Shock-Induced Separation. NACA TN 3454, 1955.
5. Love, Eugene S.: Pressure Rise Associated with Shock-Induced Boundary-Layer Separation. NACA TN 3601, 1955.
6. Burgess, Warren C., Jr., and Seashore, Ferris L.: Criteria for Condensation-Free Flow in Supersonic Tunnels. NACA TN 2518, 1951.



C-47486

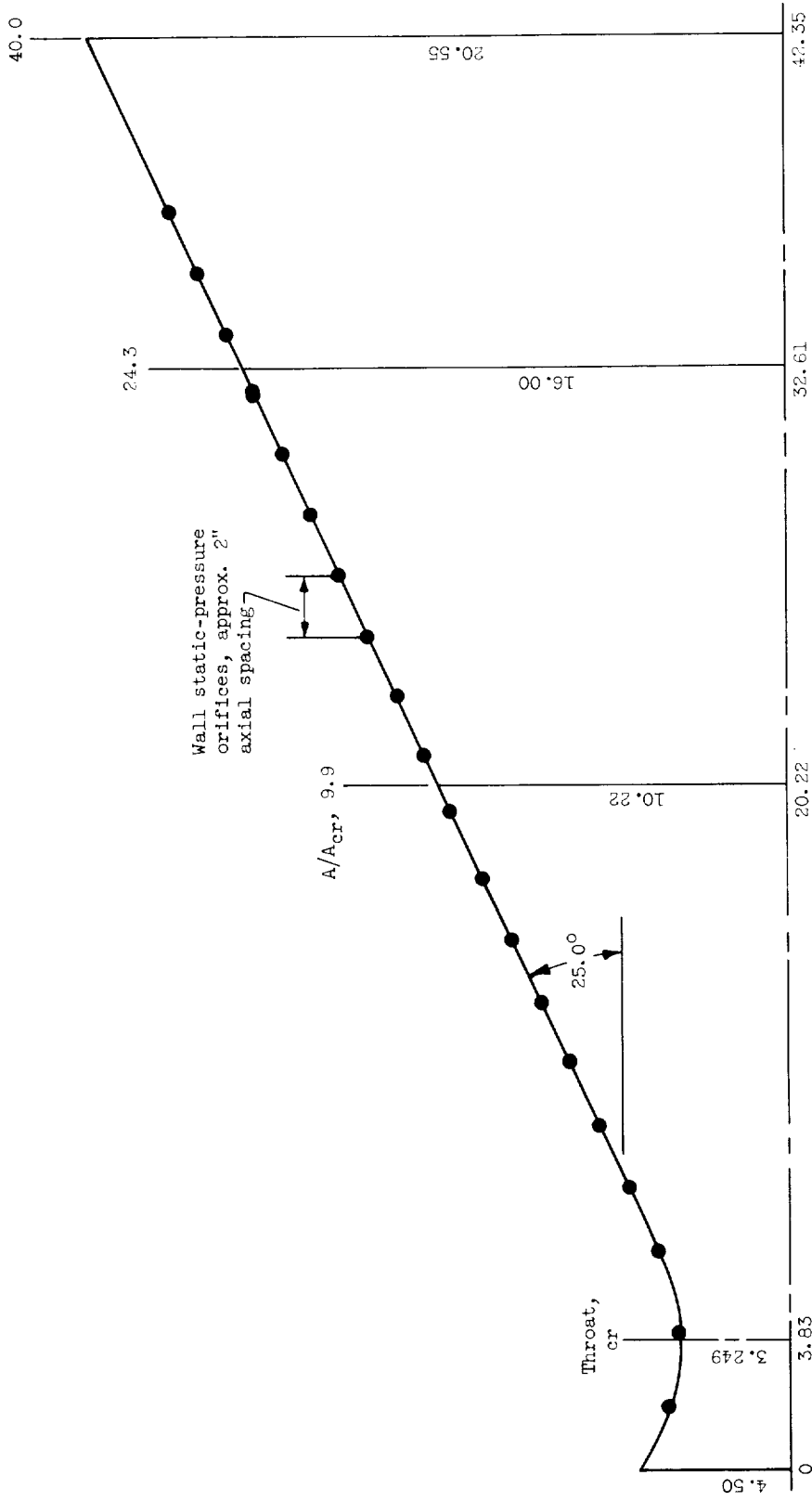
(a) Photograph of 25° nozzle installed in test rig.

Figure 1. - Nozzle configuration details.



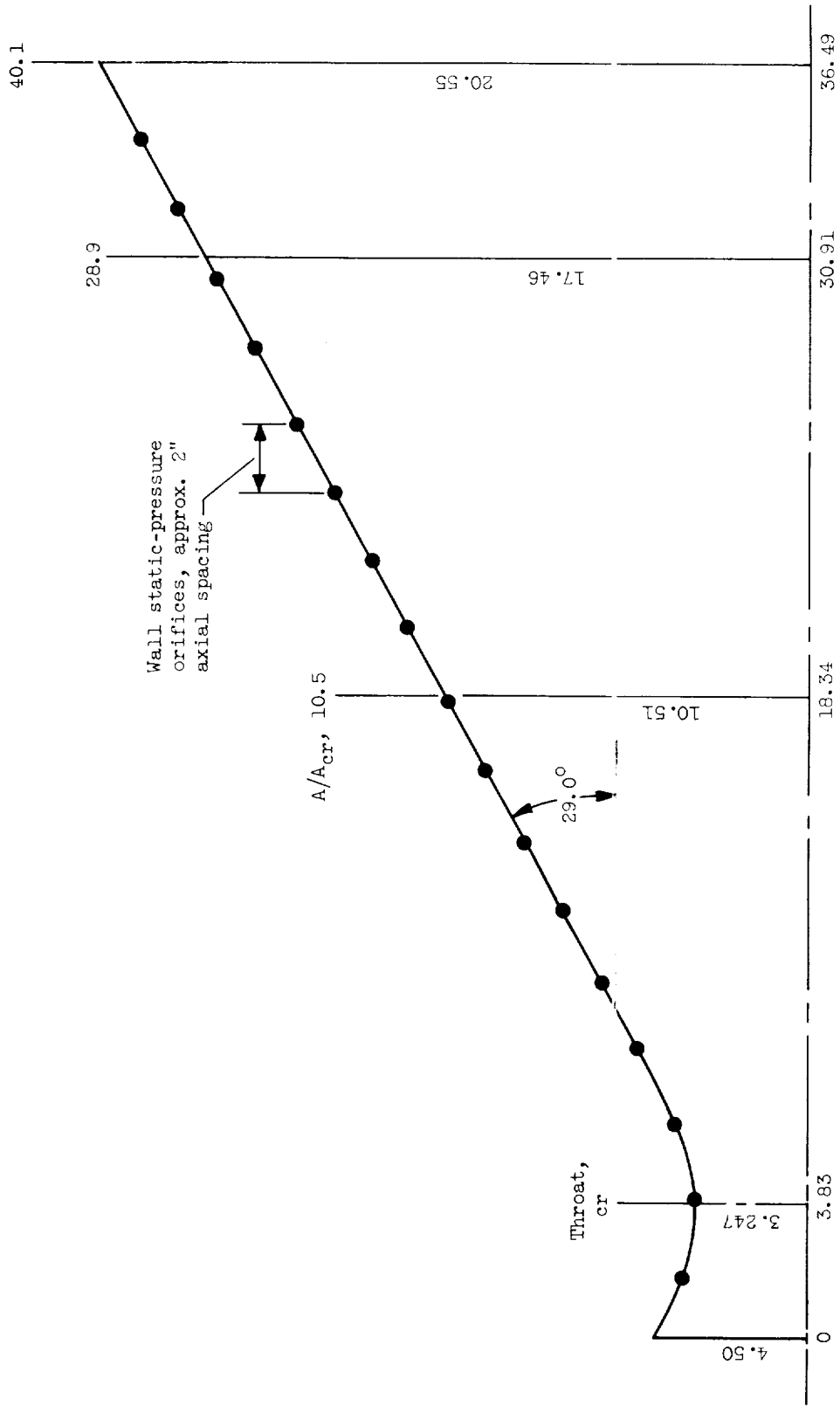
(b) Nozzle half-angle, 15.3° (dimensions in inches).

Figure 1. - Continued. Nozzle configuration details.



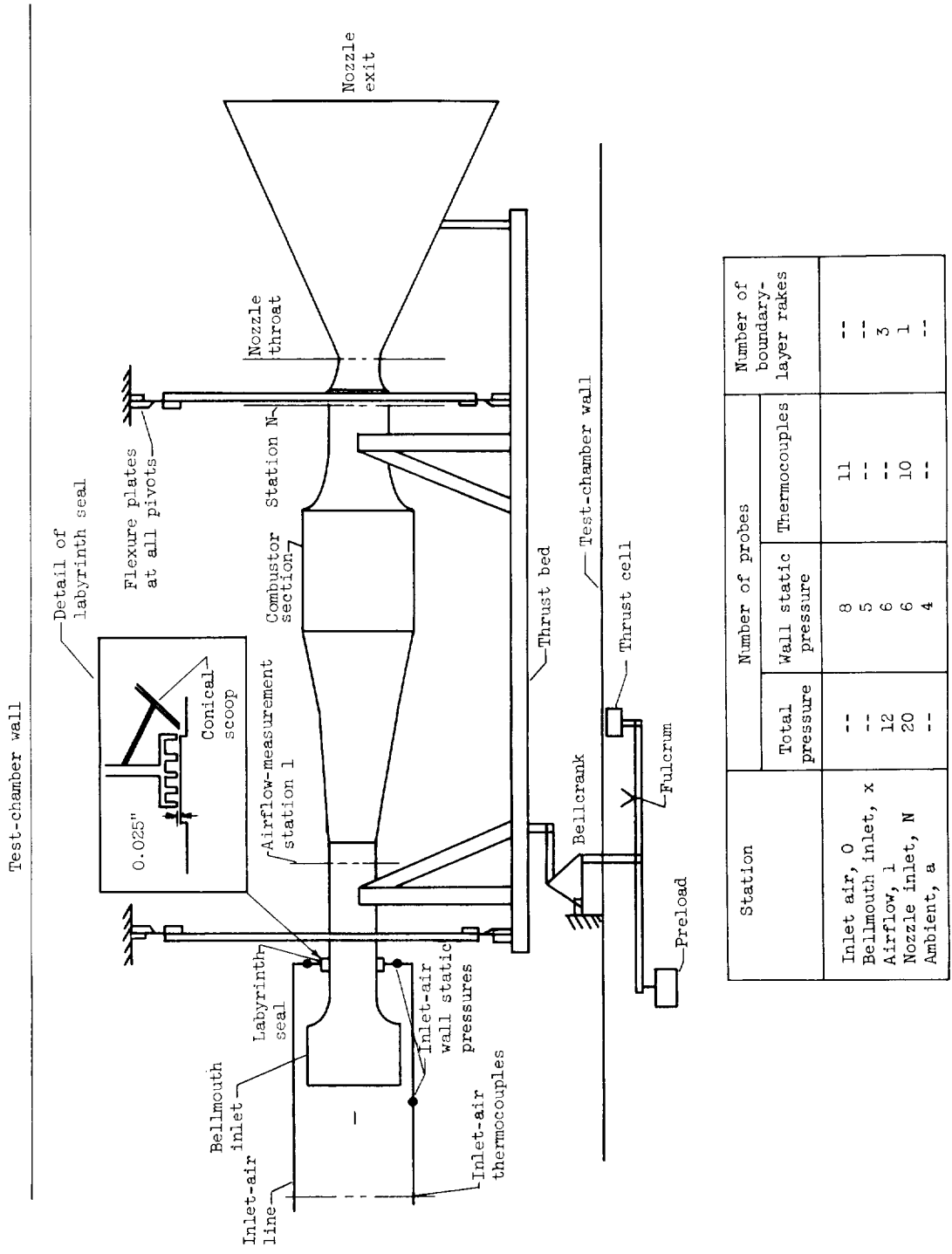
(c) Nozzle half-angle, 25.0° (dimensions in inches).

Figure 1. - Continued. Nozzle configuration details.



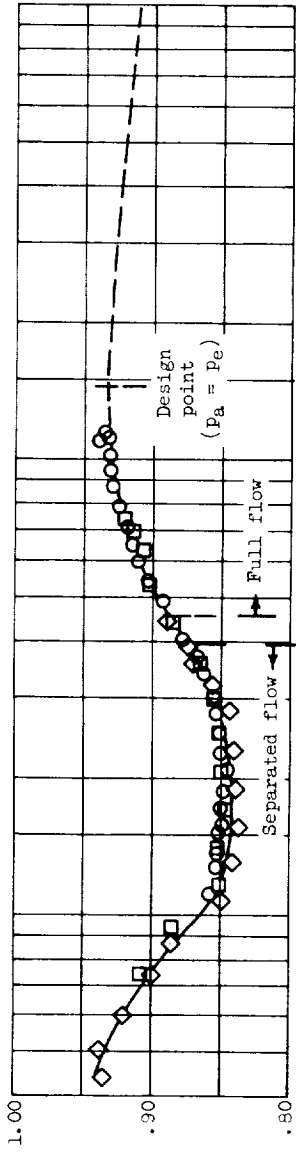
(d) Nozzle half-angle, 29.0° (dimensions in inches).

Figure 1. - Concluded. Nozzle configuration details.

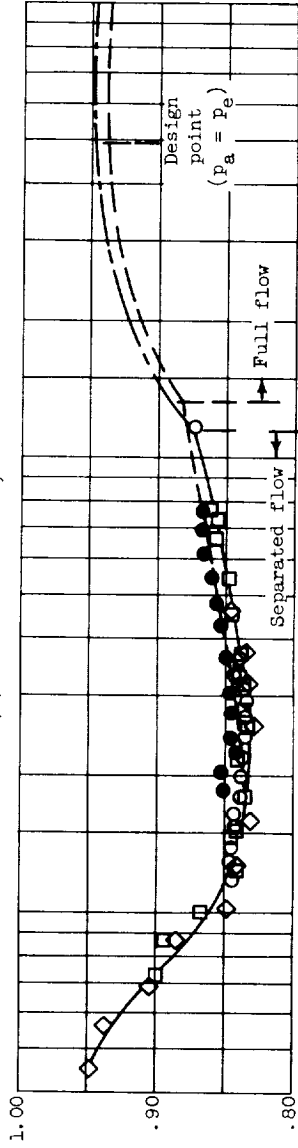


Station	Number of probes		Number of boundary-layer rakes
	Total pressure	Wall static pressure	
Inlet air, 0	--	8	--
Bellmouth inlet, x	--	5	--
Airflow, 1	12	6	3
Nozzle inlet, N	20	6	1
Ambient, a	--	4	--

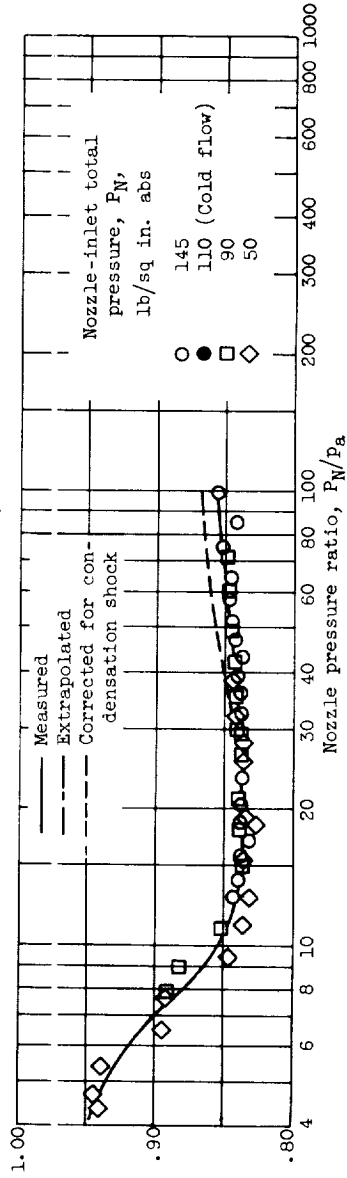
Figure 2. - Schematic diagram of nozzle test rig showing instrumentation locations.



(a) Nozzle area ratio, 10.5.



(b) Nozzle area ratio, 28.9.



(c) Nozzle area ratio, 40.1.

Figure 3. - Nozzle thrust performance with and without condensation shock. Nozzle divergence angle, 29°.

E-481

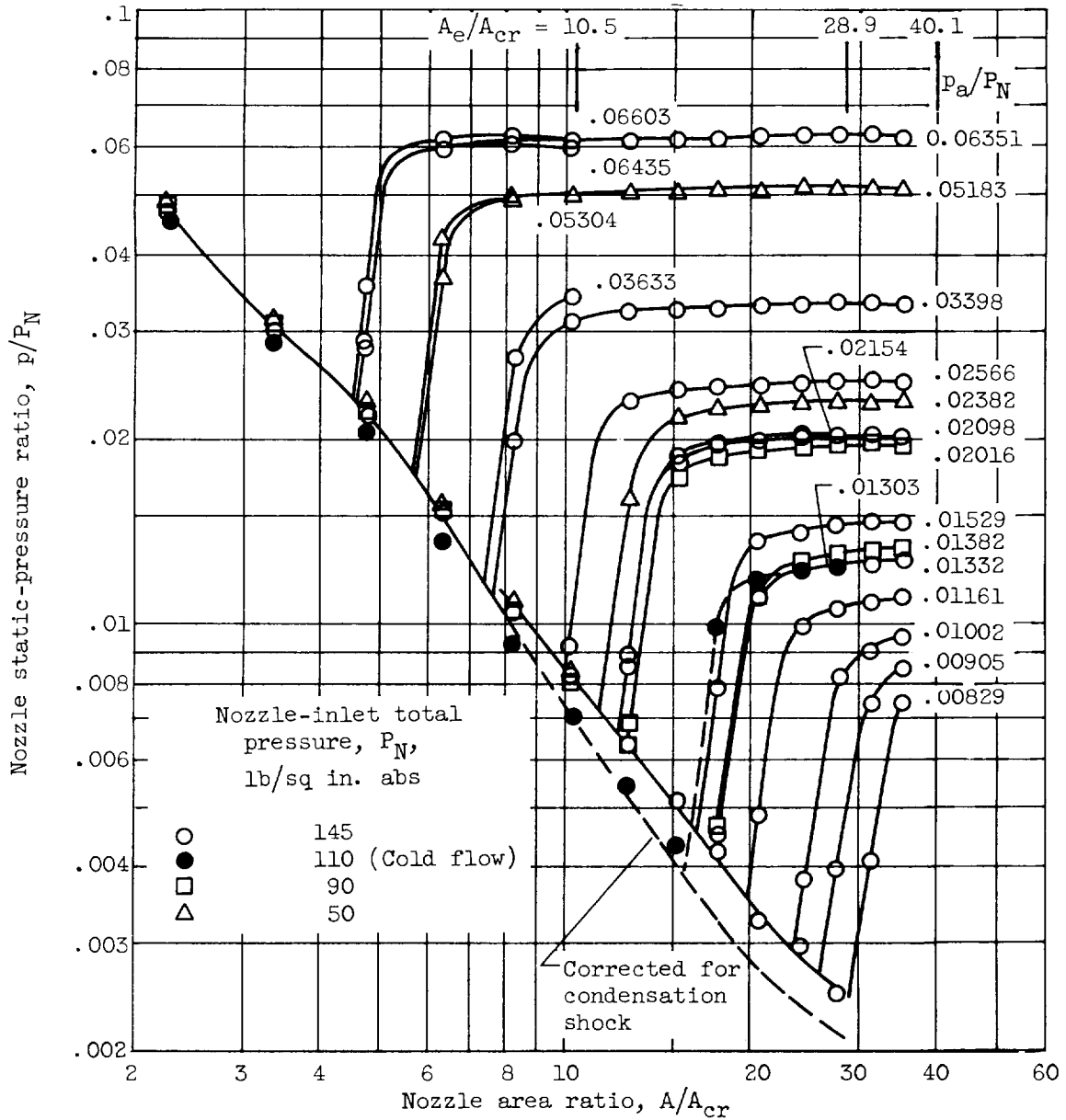


Figure 4. - Static-pressure distribution of 29°-divergence-angle nozzle.

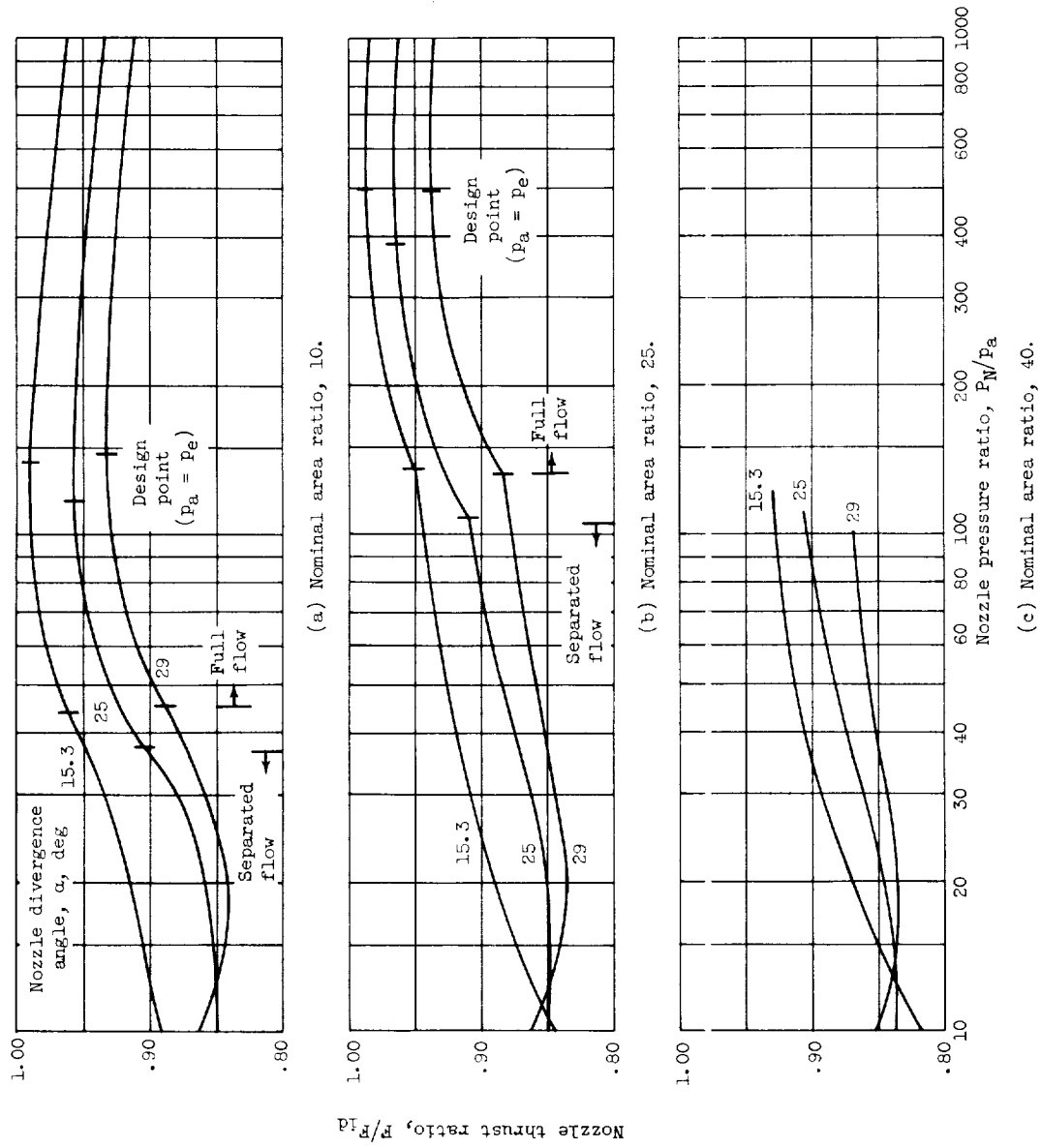


Figure 5. - Variation of nozzle thrust ratio with nozzle pressure ratio for all configurations (corrected for condensation shock).

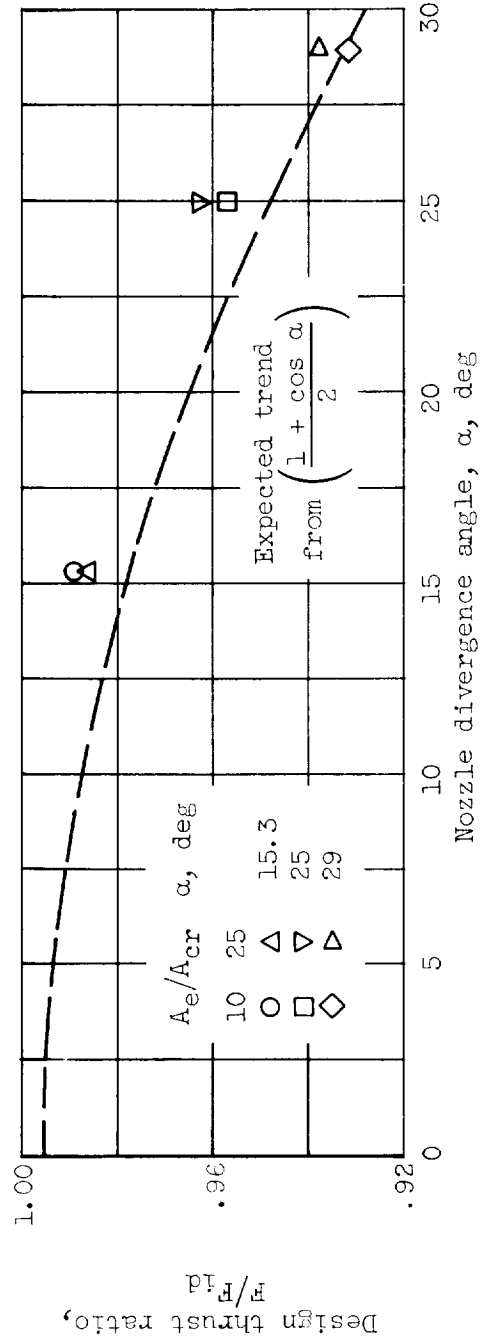


Figure 6. - Design thrust ratio as function of nozzle divergence angle.

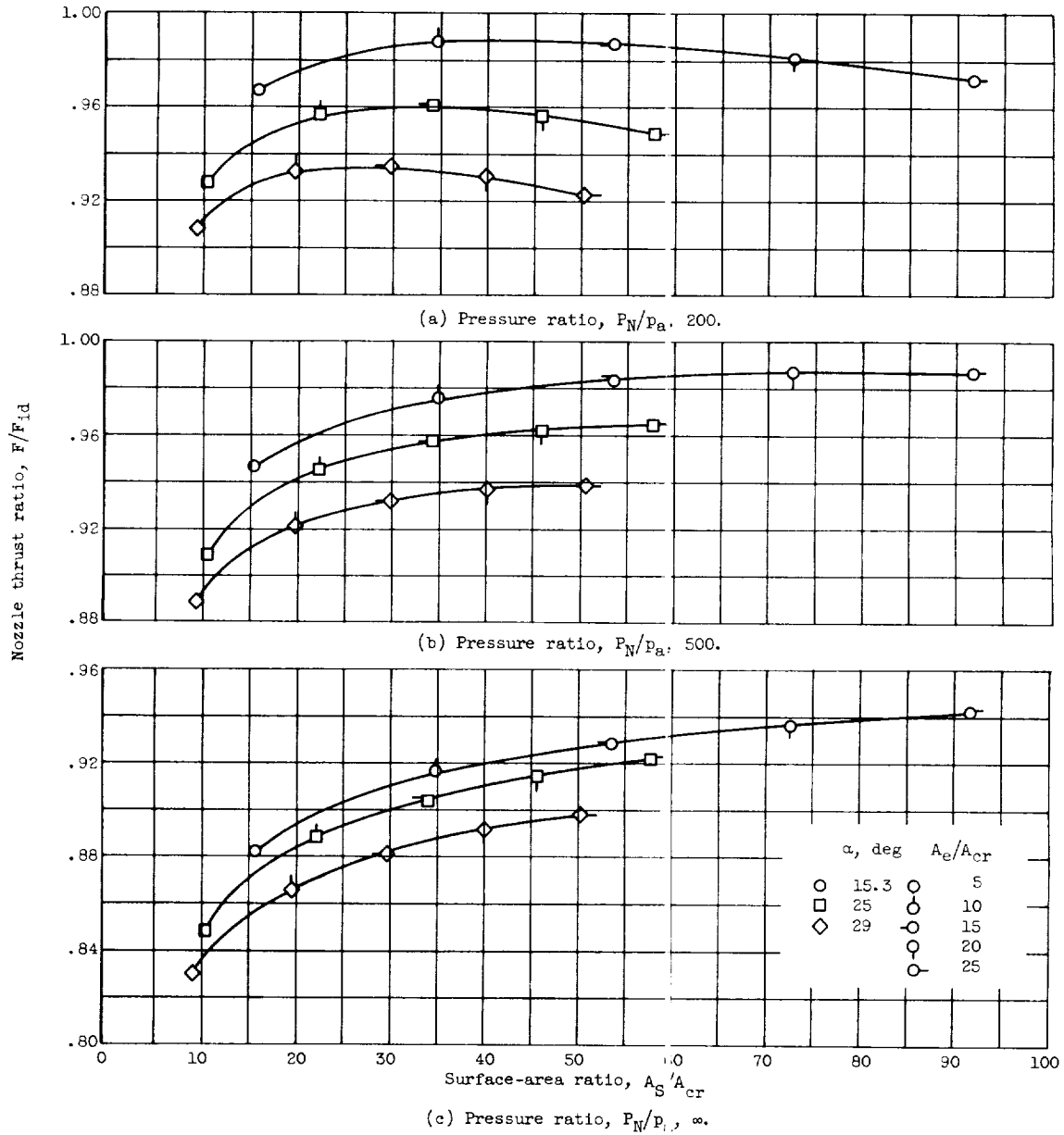


Figure 7. - Comparison of different-divergence-angle nozzles on basis of thrust per unit surface area.

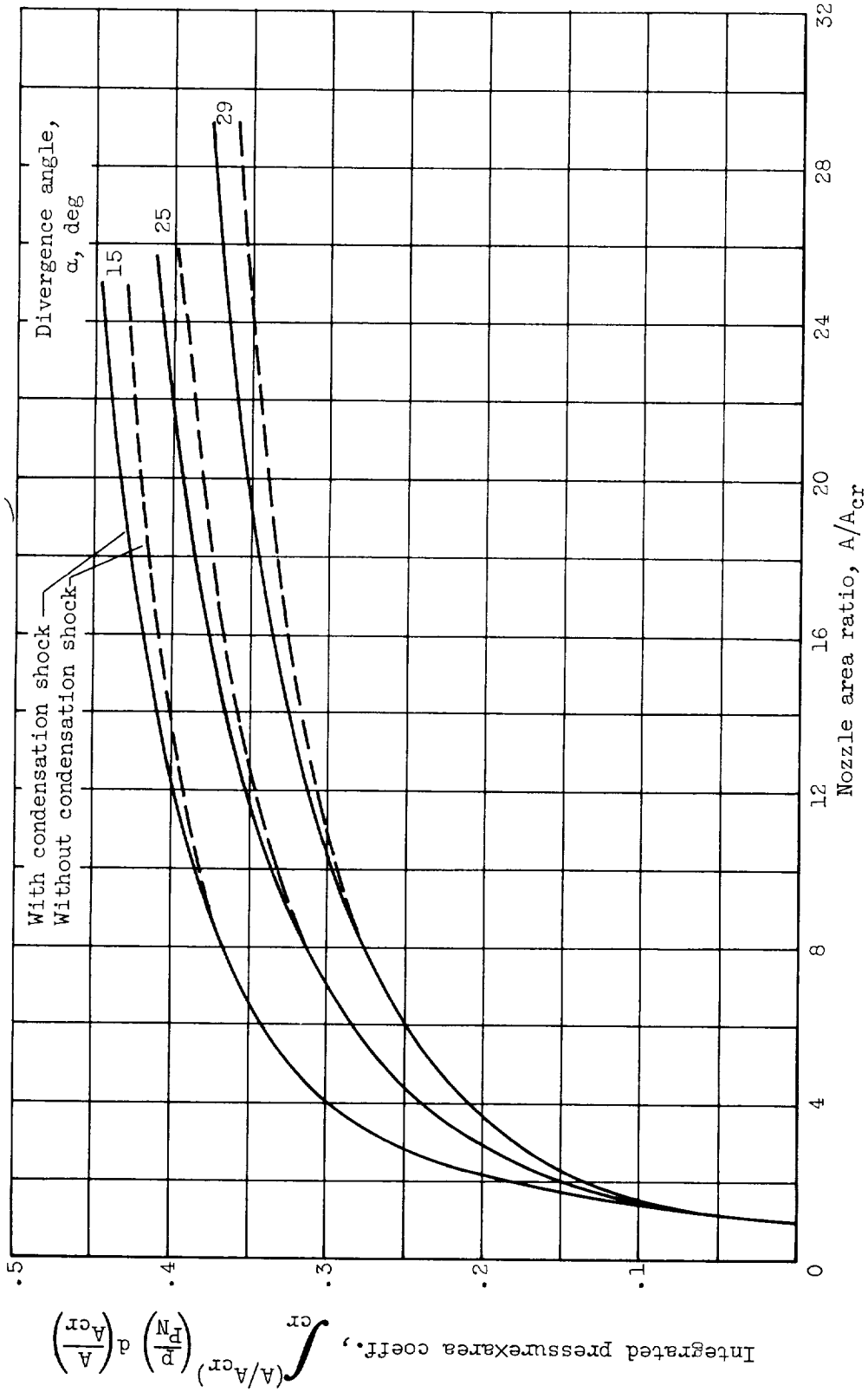


Figure 8. - Integrated pressure times area coefficient before separation as function of nozzle area ratio.

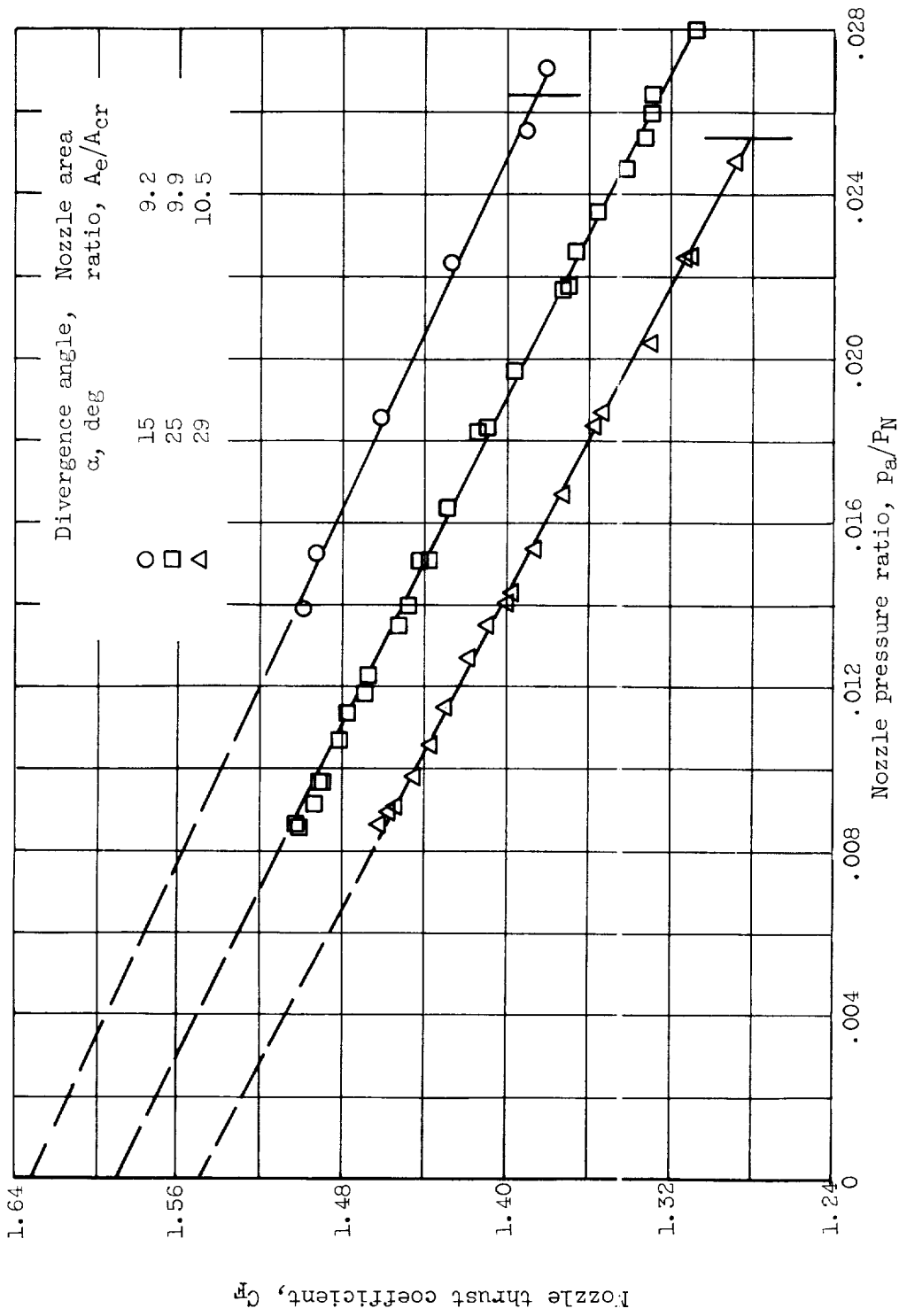


Figure 9. - Variation of nozzle thrust coefficient with nozzle pressure ratio from full flow to zero ambient pressure. Nominal nozzle area ratio, 10. (Actual data with condensation shock.)

E-481

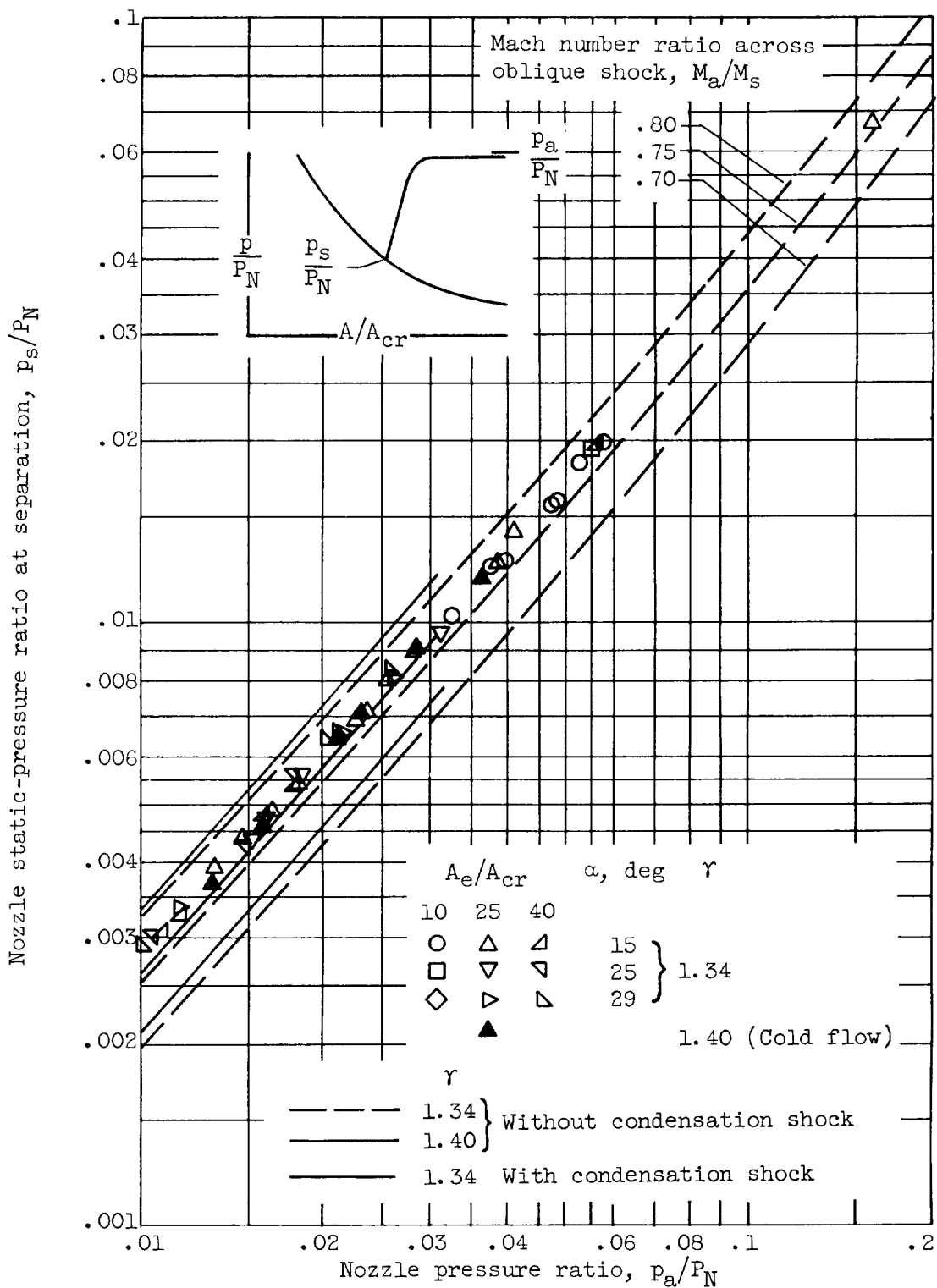


Figure 10. - Correlation of nozzle static-pressure ratio at separation with nozzle pressure ratio.

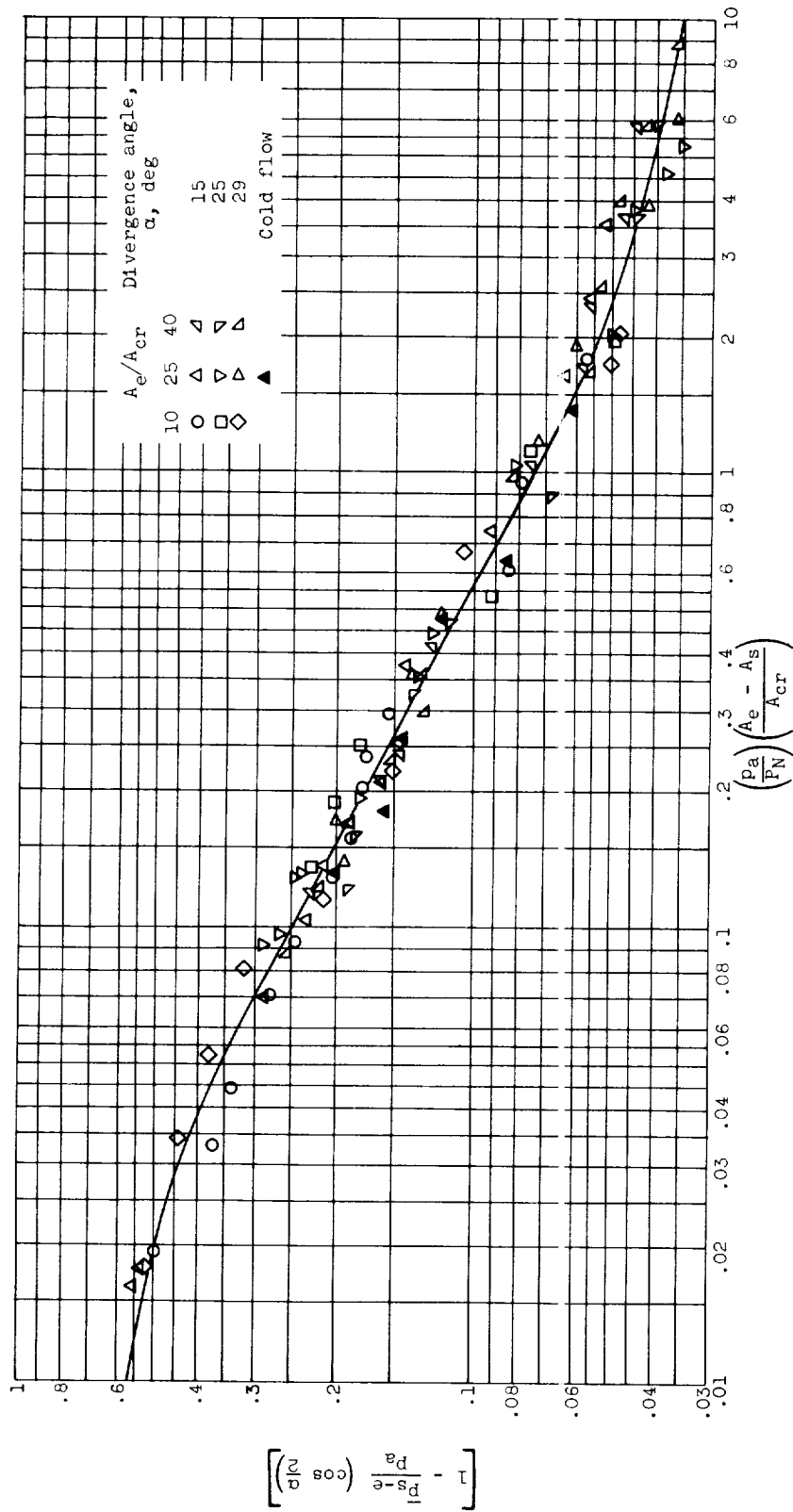
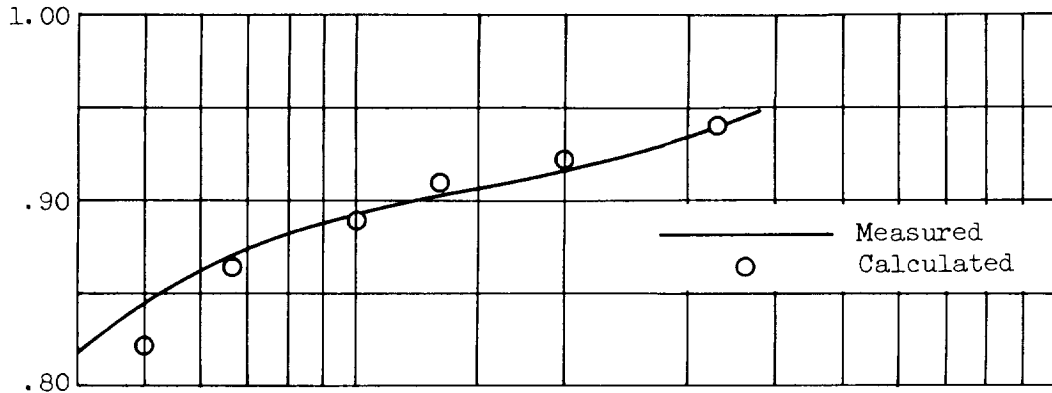
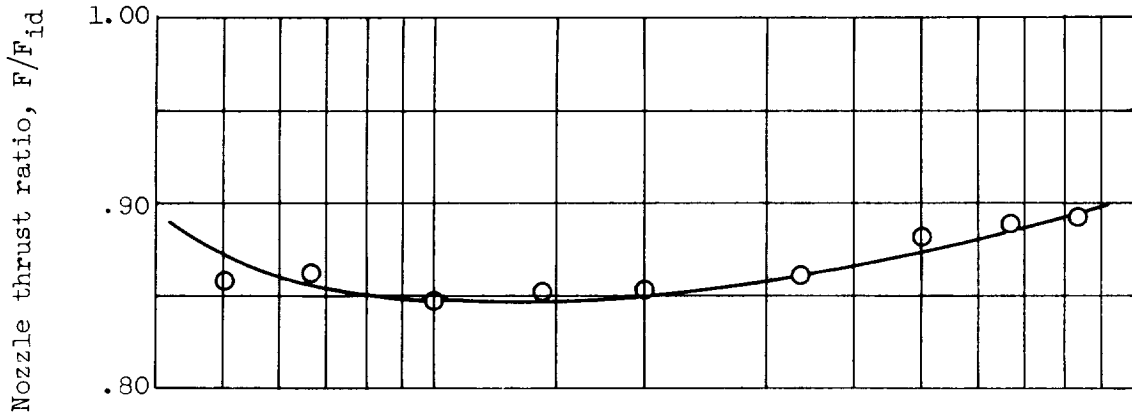


Figure 11. - Correlation of average static pressure downstream of separation with various nozzle parameters.

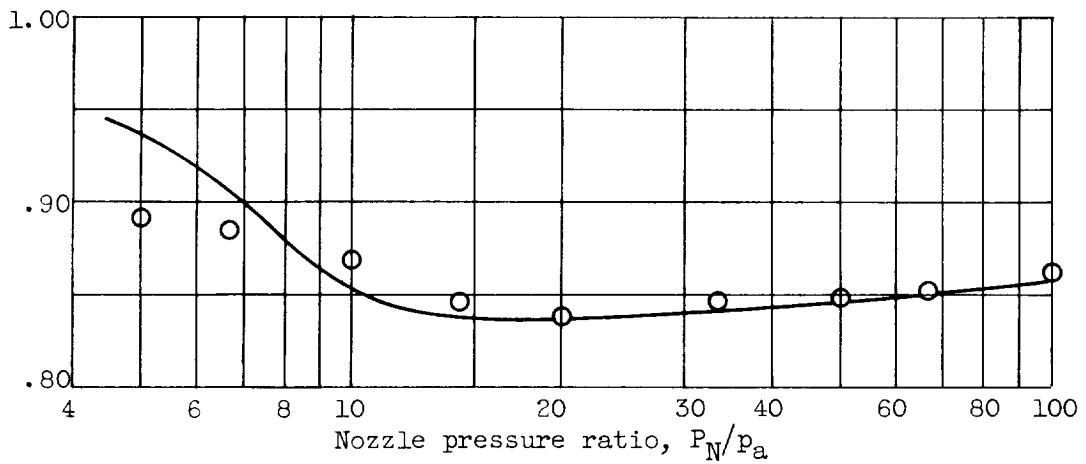
E-481



(a) Divergence angle, 15.3° ; area ratio, 9.2.



(b) Divergence angle, 25° ; area ratio, 24.3.



(c) Divergence angle, 29° ; area ratio, 40.1.

Figure 12. - Comparison of calculated and measured thrust ratios.

